

Supporting Information

A GLUT1 Inhibitor-Based Probe Significantly Ameliorates the Sensitivity of Tumor Detection and Diagnostic Imaging

Shengnan Liu^{a*}, Weijie Song^{a, b}, Yujun Cui^{a, c}, Ziru Sun^{a, d}, Zhenhua Huang^a, Qingzhi Gao^{a*}

^a Institute of Molecular Plus, Tianjin Key Laboratory for Modern Drug Delivery & High-Efficiency, School of Pharmaceutical Science and Technology, Tianjin University, 92 Weijin Road, Nankai District, Tianjin 300072, P. R. China

^b Tianjin Medical University Cancer Institute and Hospital, National Clinical Research Center for Cancer, West Huanhu Road, Hexi District, Tianjin 300060, P. R. China

^c Transplantation Center, Tianjin First Central Hospital, 24 Fukang Road, Nankai District, Tianjin 300192, P. R. China

^d Department of Biology, Gudui BioPharma Technology Inc., 5 Lanyuan Road, Huayuan Industrial Park, Tianjin 300384, P. R. China

*Corresponding Authors:

S. Liu* E-mail: shengnan_liu@tju.edu.cn

Q. Gao* E-mail: qingzhi@tju.edu.cn

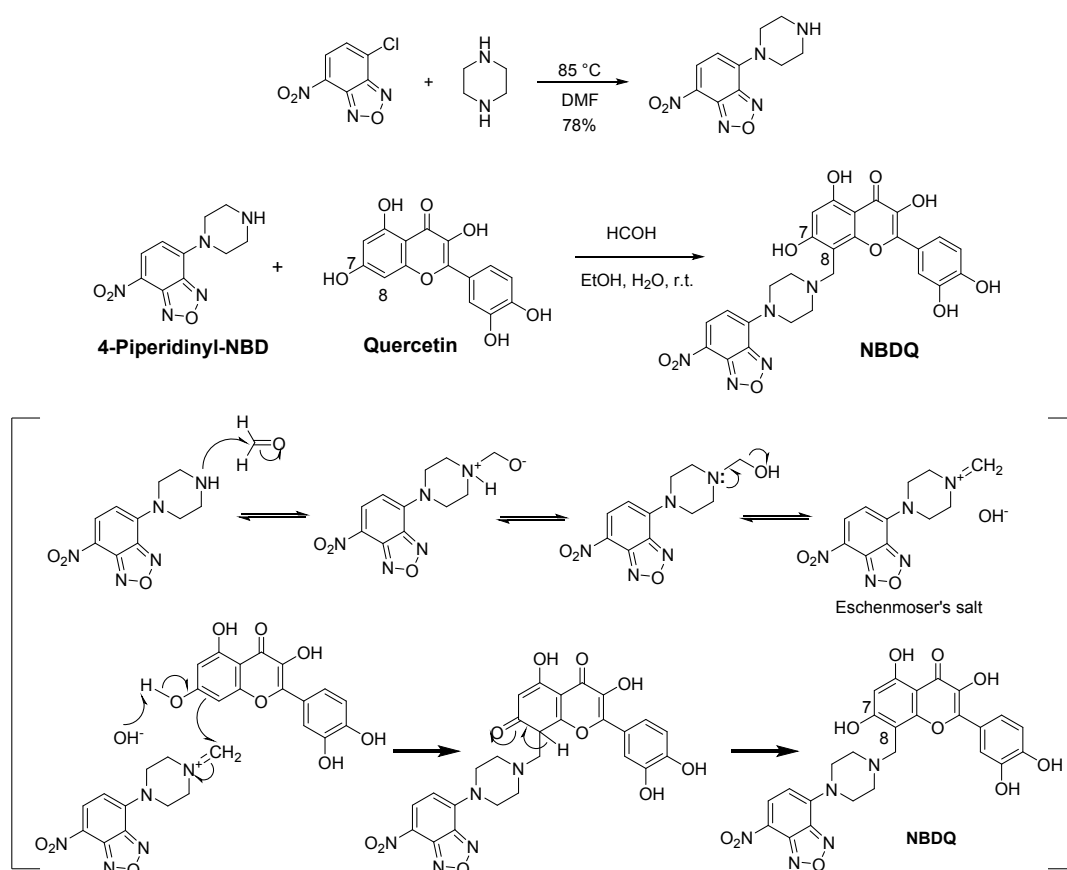
Table of Contents

1. General	S2
2. Chemistry	S2-S3
Scheme S1: Synthetic method of NBDQ.	
3. Analytical Data of the Compounds	S4-S5
Figure S1: ¹ H NMR spectrum of NBDQ	
Figure S2: ¹³ C NMR spectrum of NBDQ	
Figure S3: IR spectrum of NBDQ	
Figure S4: HRMS spectrum of NBDQ	
4. Photophysical Properties of the Probes	S6
Figure S5: UV-vis spectra of NBDQ	
Figure S6: Excitation spectra of NBDQ	
5. Biological Experimental Procedures	S7-S9
Cell lines and cell culture, Erythrocytes Isolation	
Cell Viability Assay	
Western Blot Analysis of GLUT1 Expression	
2-Deoxyglucose (2DG) Uptake Inhibition	
Competition with GLUT1 Inhibitors	
Confocal Fluorescence Imaging	
Flow Cytometry-based Tumor Cell Detection	
<i>In Vivo</i> Tumor Imaging	
6. Biological Assay Results	S10-S12
Figure S7: 2-NBDG uptake and accumulation in A549 cells.	
Figure S8: Cytotoxicity of Quercetin and NBDQ in Different Cell Lines.	
Figure S9: Known Inhibitors used for 2-DG Uptake Inhibition and Competition Assay	
Figure S10: 2-Deoxyglucose (2DG) Uptake with Inhibitor Combination in Human Erythrocyte.	
7. GLUT1 Inhibition Mechanism and Molecular Basis	S12-S16
Figure S11: Molecular dynamics simulations of hGLUT1 with GLUT1 inhibitor.	
Figure S12: Root mean square deviation (RMSD) for NBDQ-bound hGLUT1.	
Figure S13: Root mean square deviation (RMSD) for Phloretin-bound hGLUT1.	
Figure S14: Root mean square deviation (RMSD) for Quercetin-bound hGLUT1.	
Table S1: Summary of 150 ns MD simulation results for NBDQ-bound hGLUT1 complex.	
Table S2: Summary of 150 ns MD simulation results for Phloretin-bound hGLUT1 complex.	
Table S3: Summary of 150 ns MD simulation results for Quercetin-bound hGLUT1 complex.	
Figure S15: Flow cytometry-based cell differentiation analysis.	
Table S4: Tm/Bkg and Tm/Org) for NBDQ and 2-NBDG treated TNBC bearing xenograft mice.	
8. <i>In Vivo</i> Fluorescence Imaging of NBDQ in A549 Xenograft Mice	S17
Figure S16: <i>In vivo</i> imaging for NBDQ treated A549 xenograft mice.	
Table S5: Tumor-to-background ration (Tm/Bkg) and tumot-to-organ ratio (Tm/Org) for NBDQ treated A549 bearing xenograft mice.	
9. <i>In Vivo</i> Efficacy Study of NBDQ in MDA-MB-468 Xenograft Mice	S18
Figure S17: <i>In vivo</i> antitumor efficacy for NBDQ treated MDA-MB-468 xenograft mice.	
10. Original Gels of the Western Blot	S18
11. References	S18-S19

1. General

Materials and Instrumentation. For chemistry, all chemicals were obtained from commercial suppliers and were used as received. If necessary, the reactions were carried out in dry solvents and under an argon atmosphere. ^1H and ^{13}C NMR spectra were recorded with a Bruker Avance 400 or 600 MHz at the School of Pharmaceutical Science and Technology of Tianjin University, PRC. Data are reported as chemical shifts (δ) in parts per million (ppm) relative to the solvent peak, and scalar coupling constants (J) are reported in units of hertz (Hz). HPLC analyses were carried out using a CXTH-LC3000 analytical and semi-preparative gradient HPLC system with a DaisoGel C18 (4.6 x 250 mm, 5 mm) and DaisoGel C18 (20 x 250 mm, 10 mm) column at room temperature. The mobile phase consisted of MeOH and H₂O, and the flow rate was 1 mL/min for analytical purification and 15 mL/min for preparative purification. Infrared spectra were recorded using a Bruker Tensor 27 FT-IR spectrometer in a KBr pellet, which was prepared by grinding the solid sample with solid KBr and applying great pressure to the dry mixture. Absorptions are reported in wavenumbers (cm^{-1}). UV-visible spectroscopic analysis was performed using a U-3900 UV-VIS spectrophotometer at room temperature with a quartz cuvette having a pathlength of 0.2 cm as a sample holder. Fluorescence spectra were measured using a Varioskan LUX multimode microplate reader (Thermo Fisher Scientific). High-resolution mass spectra (HRMS, m/z) were recorded on a Bruker MicroTOF spectrometer in positive mode (ESI+).

2. Chemistry



Scheme S1. Synthetic route and hypothesized mechanism for regioselective production of NBDQ via quercetin-based mannich coupling.

Preparation of 4-piperidinyl-NBD. To a 25 mL round-bottomed flask was added 199.5 mg (0.5 mmol) of 4-chloro-7-nitrobenzo-2,1,3-oxadiazole (4-Cl-NBD) and 172.2 mg (2 mmol) of piperazine. Then DMF was added. The reaction was stirred for 4 h at 85 °C. The mixture was then evaporated and the residue was purified with column chromatography (silica gel, dichloromethane/ethyl acetate = 6 : 1, v/v). 4-piperidinyl-NBD was obtained as a red solid (97.6 mg), yield: 78%. ¹H NMR (400 MHz, DMSO-*d*₆): δ 8.47–8.45 (d, *J* = 8.00 Hz, 1H), 6.66–6.64 (d, *J* = 8.00 Hz, 1H), 4.08 (s, 4H), 2.95–2.93 (t, *J* = 4.00 Hz, 4H). EI-MS *m/z* (M⁺) calcd 249.08, found 249.02.

Preparation of NBDQ. To a suspension of quercetin (0.35mmol) in EtOH (5mL) was added 37 percent (wt) formaldehyde in H₂O (0.35mmol) and amine (0.35mmol). The resulting suspension was allowed to stir for 16h. NBDQ as desired product was isolated via vacuum filtration as a yellowish solid. yield: 71%. ¹H NMR (400 MHz, DMSO-*d*₆) δ 8.44 (d, *J* = 8.9 Hz, 1H), 7.74 (s, 1H), 7.61 (d, *J* = 8.2 Hz, 1H), 6.89 (d, *J* = 8.4 Hz, 1H), 6.64 (d, *J* = 9.2 Hz, 1H), 6.27 (s, 1H), 4.14 (s, 4H), 3.85 (s, 2H), 2.6–2.85 (m, 4H). ¹³C NMR (100 MHz, DMSO-*d*₆): δ 176.30, 163.22, 154.75, 145.65, 145.37, 145.18, 145.12, 136.70, 136.06, 122.71, 121.47, 120.51, 116.04, 104.03, 103.37, 101.34, 98.14, 52.41, 49.70, 48.95. IR (KBr): 3416, 1653, 1613, 1546, 1498, 1442, 1293, 1246, 1176, 1131, 1111, 1046, 997, 802 cm⁻¹. HRMS (ESI) *m/z*: 562.1223 [M-1]⁺, calcd for C₂₆H₂₁N₅O₁₀ (M-1)⁺: 562.1228.

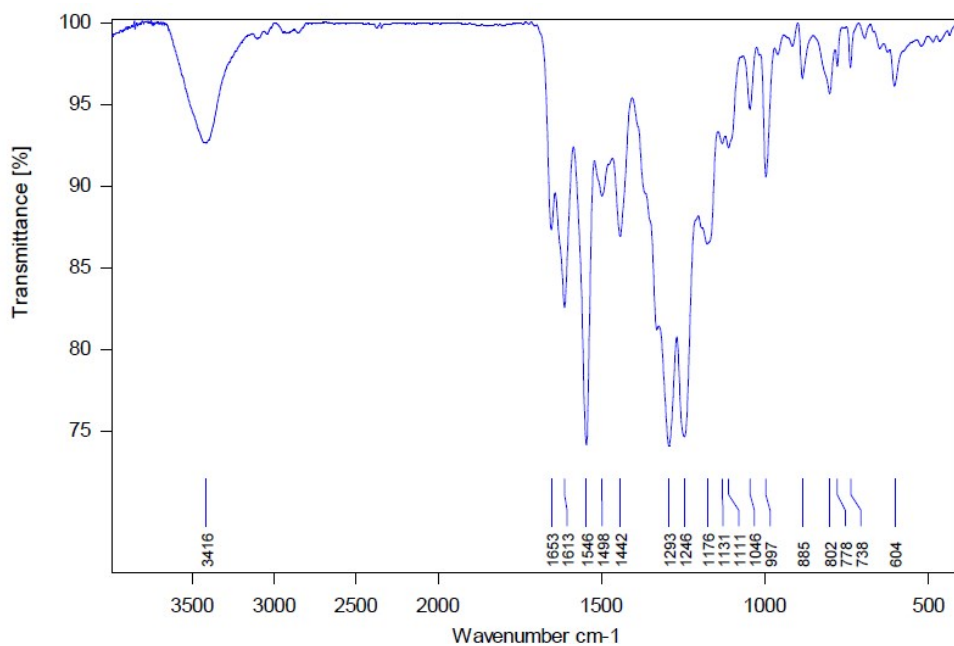


Figure S3. IR (KBr) spectrum of NBDQ.

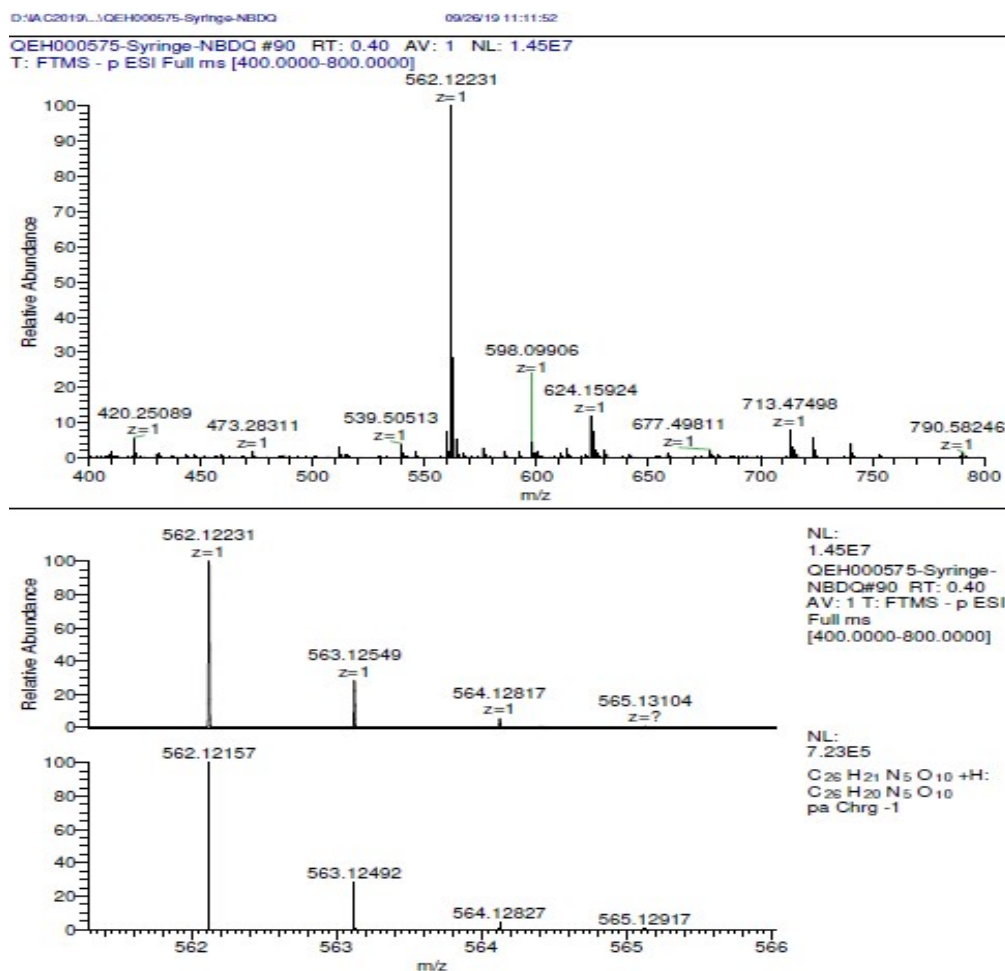


Figure S4. HRMS spectrum of NBDQ.

4. Photophysical Properties of the Probes

UV-visible and Fluorescence Spectroscopy. The UV-visible spectroscopic analysis and fluorescence spectroscopic studies were performed by using a Varioskan LUX multimode microplate reader (Thermo Fisher Scientific) to acquire the absorption, excitation and emission spectra of the probe. First, 1 mM stock solutions of NBDQ in DMSO (Tokyo Chemical Industry) were prepared by vortexing followed by ultrasonication for 15 min and were shaken by hand during the ultrasound treatment. The stock solution was further diluted with PBS (pH=7.0) to different concentrations as working solutions. A 96-well black polystyrene microplate (Thermo Fisher) was used for fluorescence measurements in the ranges of $\lambda_{ex} = 200\text{--}550$ and $\lambda_{em} = 400\text{--}750$ nm.

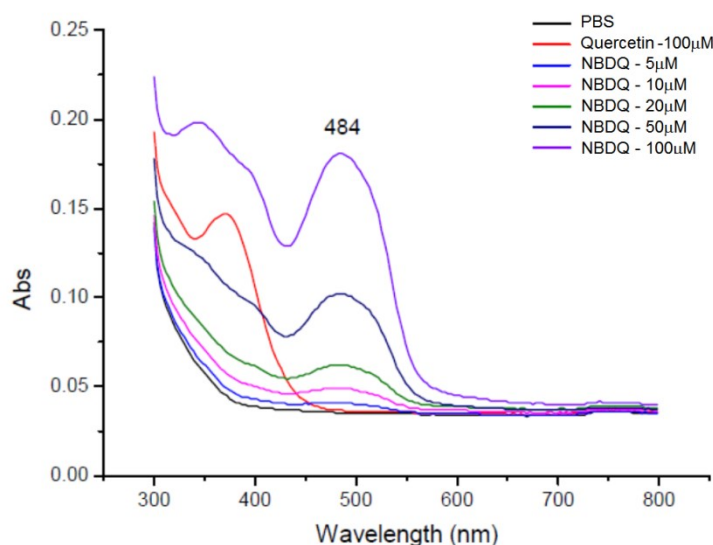


Figure S5. UV-vis spectra of NBDQ.

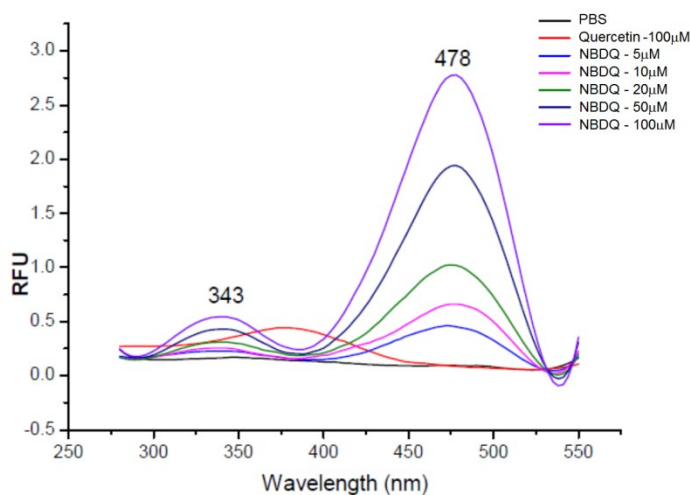


Figure S6. Excitation spectra of NBDQ.

5. Biology Experimental Procedures

Purchase Details of the Fatal Bovine. Heat deactivated fetal bovine serum (FBS) was purchased from Gibco and was used as 10% solution of corresponding cell culture medium.

Cell Lines and Cell Culture. Human bronchial epithelium cell BEAS-2B, human non-small-cell lung cancer cell A549 and human mammary epithelial cell line MCF10A were purchased from ATCC. Human triple negative breast cancer cells MDA-MB-468 was a gift from Tianjin Medical University Cancer Institute & Hospital. A549 cells were cultured at 37°C in RPMI 1640 medium (High Glucose; Gibco, Invitrogen), and supplemented with 10% fetal bovine serum (FBS; Gibco, Invitrogen) and 1% penicillin/streptomycin solution (Gibco, Invitrogen) in humidified atmosphere with 5% CO₂. BEAS-2B, MCF 10A and MDA-MB-468 cells were cultured in Dulbecco's modified Eagle's medium (DMEM 1x, High Glucose; Gibco, Invitrogen) at 37°C with 10% fetal bovine serum and 100 U.mL⁻¹ penicillin-streptomycin under a 5% CO₂ environment.

Erythrocytes Isolation. Human venous blood from healthy volunteers was obtained from Tianjin Medical University Cancer Institute & Hospital. This study was approved by the Ethics Committee of Tianjin Medical University Cancer Institute and Hospital, and all protocols conformed to the Ethical Guidelines of the World Medical Association Declaration of Helsinki. Signed informed consent was obtained from each participating individual prior to participation in the study. Blood samples were collected from two healthy human subjects into heparinized blood collection tubes. Rat blood samples were collected and treated with 3.2% sodium citrate to avoid coagulation. Erythrocytes from humans and rats were isolated following the protocol described below: The whole blood samples were centrifuged at 2000 × g for 5 min at 4°C. After that the supernatant plasma was aspirated and the erythrocyte pellet was washed with cold PBS, then centrifuged at 2000 × g for 5 min at 4°C. This step was repeated two more times for a total of 3 washes of the erythrocytes, and the isolated pure erythrocytes were stored in PBS at 4°C for immediate use.

Fluorescence Spectroscopy. For fluorescence spectrum analysis, NBDQ was dissolved in dimethyl sulfoxide (Tokyo Chemical Industry) to create a stock solution at the concentration of 20 mM by vortex for 1 minute. The resultant solution was then subjected to further dilution with PBS to 100 μM working solution. The excitation and emission spectra of the NBDQ compound was detected by microplate reader (Thermo Varioskan LUX Multimode Microplate Reader). A corning 96 well black flat bottom polystyrene microplate was used for fluorescence recording in the ranges of $\lambda_{\text{ex}}=280\text{--}550$ and $\lambda_{\text{em}}=450\text{--}750$ nm. The data was statistically analyzed using OriginPro 8.5.

Cell Viability Assay. The BEAS-2B, A549, MCF10A and MDA-MB-468 cells were seeded at a density of 5,000 cells per well in a flat bottomed 96-well using 100 μL of culture medium on day 0. On day one, cells were treated with increasing doses of NBDQ and quercetin for 72h, keeping a final concentration of 0.5% DMSO. 100μL of culture medium was removed. MTT (Sigma-Aldrich) was

added to each well at the final concentration of 0.83 mg/mL and incubated for 4 h. Cells were lysed by MTT lysis buffer (15% SDS, 0.015M HCl) and the uptake of MTT was measured at 490 nm using a multi-well-reading UV-Vis spectrometer. For each compound, cell survival rates were expressed as the relative percentage of absorbance compared to controls without drug. Experiments were performed in four replicates (4 wells of the 96-well plate per experimental condition) and repeated for three times.

Western Blot Analysis of GLUT1 Expression. Cells were washed twice with ice-cold $1 \times$ PBS and lysed using RIPA lysis buffer (Sigma) supplemented with complete MINI protease inhibitor tablets (1 per 10 mL, Roche) (Roche) and PhosSTOP phosphatase inhibitor tablets (1 per 10 mL, Roche). Lysates were sonicated and then centrifuged at 12000 rpm at 4 °C for 10 min. Total protein concentration was quantified with pierce BCA protein assay kit (Thermo Scientific). 10 μ g of total cell protein were loaded onto 10% SDS-PAGE and then transferred to a microporous polyvinylidene difluoride (PVDF) membrane. Western blotting was performed using Polyclonal anti-GLUT1 antibody (1:2000) (ab652, Abcam), anti- β -actin antibody (Sigma), and goat anti-rabbit IgG-peroxidase conjugate as the secondary antibody. The detection of the proteins was carried out using horseradish peroxidase (HRP) as a chemiluminescent substrate.

2-Deoxyglucose (2DG) Uptake Inhibition. Human erythrocytes were plated at 5×10^6 /well in 96-well plates and washed 3 times with 3 mL wash Krebs Ringer Phosphate HEPES (KRPH) buffer (118 mM NaCl, 5 mM KCl, 1.3 mM CaCl_2 , 1.2 mM MgSO_4 , 1.2mM KH_2PO_4 , 30mM HEPES, pH 7.4). Treatment groups include: KRPH buffer with 1 mM 2-deoxyglucose (Sigma) as a control, KRPH buffer with 1 mM 2-deoxyglucose, quercetin, cytochalasin B, phloretin and NBDQ (0.1-100 μ M). Treated erythrocytes were incubated at 37°C for 1 hour. After incubation, all samples were washed in cold PBS for 3 times. Erythrocytes were lysed in 10 mM Tris-HCl buffer (pH 8.0) with 0.5% triton X-100 at 80 °C for 15 minutes and centrifuged at $15000 \times g$ for 20 minutes at 4 °C and the supernatant was transferred to a new tube. Glucose uptake assay was performed with 2-Deoxyglucose (2DG) Uptake measurement kit (Cosmo Bio Co. Ltd., Tokyo, Japan) following the manufacturer's instructions.

Competition with GLUT1 Inhibitors. MDA-MB-468 cells were seeded in a Corning 96 well black flat bottom polystyrene microplate and incubated overnight until cells reached appropriate confluence. The growth medium was aspirated and cells were washed twice with PBS and incubated in glucose-free medium for 2 hours. Then increasing concentrations of phlorizin (0-200 μ M, Sigma) or cytochalasin B (0-20 μ M, Sigma) was added. After 30 min of treatment of the inhibitors at 37°C, NBDQ solution (25 and 50 μ M) was added and cultured at 37°C for another 30 min. At the end of the treatment, cells were washed 3 times with cold PBS and subjected to fluorescence detection. The fluorescence intensity was recorded using Varioskan LUX Multimode Microplate Reader. For quantitative purposes, cells were subjected to the MTT-mediated cell viability assay to normalize the fluorescence levels according to the number of living cells.

Confocal Fluorescence Imaging. Testing cells were aliquoted into 6-well plates. Confocal

experiments were started by the addition of 50 nM of NBDQ or 500 nM of 2-NBDG into each sample. After 30 min of incubation at 37 °C, the cells were washed 3 times with cold PBS and seeded in glass bottom dish (NEST, China). The chamber slides were then mounted and sealed for confocal microscopic analysis using an Olympus FV1000-IX81 confocal-laser scanning microscope with 488 nm excitation through a 100 × 1.4 NA oil immersion objective lens.

Flow Cytometry-based Tumor Cell Detection. 4 mM DMSO solution of NBDQ was diluted with RPMI 1640 medium to 50 μM cell staining solution. Filtration was performed using a 0.22 μm pore filter before use. High GLUT1 expression A549 cancer cells and low expression normal BEAS-2B cells were used for the experiments. Single-cell suspension of both A549 and BEAS-2B containing 1×10^6 cells/tube were prepared and cells were collected by centrifugation at 8000 rpm for 2 min. The supernatant was removed and cells were treated with the staining solution (0.5 mL/tube) and incubated at 37 °C for 30 min. Staining solution was removed after centrifugation at 8000 rpm for 2 min and cells were washed twice with ice-cold PBS (0.5 mL x 2). After the labeling process, test samples were prepared as cell suspension in 0.3 mL PBS and used for flow cytometry analysis. Unlabeled A549 and BEAS-2B cells were prepared following the same process without staining and assigned as negative control group (A549-control, BEAS-2B-control). NBDQ labeled A549 and BEAS-2B cells were regarded as positive control group (A549-positive and BEAS-2B-positive). A mixture of NBDQ labeled A549 and BEAS-2B cells with different ratio of A549 cells to BEAS-2B cells were prepared (A:B = 1:1, 1:2, 1:4) and used for flow cytometry-based differentiation analyses.

In Vivo Tumor Imaging. *In vivo* fluorescence imaging was performed with a Xenogen IVIS small animal imaging system. The 465 nm excitation and 580 nm emission filter set was used for acquiring both 2-NBDG and NBDQ probe fluorescence *in vivo*. The fluorescent images were captured by a low noise CCD camera. For each experiment, 4 to 6 week-old athymic female nude mice (Beijing Vital River Laboratory Animal Technology Co., Ltd.) (n=3) were used. Human triple-negative breast cancer and human non-small cell lung cancer A549 cells (8×10^6) were subcutaneously inoculated into the right flank region next to the fore- or hindlimb, or the lower back of the nude mice. Mice bearing 5-10 mm-diameter tumors were tail intravenously injected with 100 μL of 1.1 mg/mL NBDQ (0.2 μmol, 0.11 mg/mice) probe and the same equimolar dosage of 2-NBDG (0.2 μmol, 0.068 mg/animal). PBS was used as a negative control. After completion of the experiment, the nude mice were sacrificed and the main organs as well as tumors were harvested. The fluorescence images of these organs were individually taken as above. All experiments were performed according to the regulation and guideline of Institutional Animal Care and Use Committee at Tianjin Medical University Cancer Institute and Hospital by following the Guide for the Care and Use of Laboratory Animals (NRC 2011). To measure the tumor-to-background ratio, ovoid regions of interest (ROI) were manually drawn over the subcutaneous tumors to measure the fluorescence intensity of tumor (FI_{tumor}), a second ROI was drawn on the contralateral site as background activity (FI_{bkg}). Tumor-to-background ratio were calculated based on the following formula:

$$\text{Tumor-to-background ratio (Tm/Bkg)} = \text{FI}_{\text{tumor}} / \text{FI}_{\text{bkg}}$$

The tumor-to-organ ratio for groups of mice (n=3) was based on the *ex-vivo* optical images of the tumor and selected main organs. Average fluorescence intensity of the selected organs (FI_{org}) was used in the following formula:

$$\text{Tumor-to-organ ratio (Tm/Org)} = \text{FI}_{\text{tumor}} / \text{FI}_{\text{org}}$$

6. Biological Assay Results

2-NBDG uptake and accumulation in A549 cells. The spectroscopic evaluation was conducted in PBS at pH 7.4 by using a Thermo Scientific Varioskan LUX multimode microplate reader. As shown in Fig. S7 and as has been reported previously,^[1] for uptakeable glucose tracer 2-NBDG, increased extracellular concentrations of 2-NBDG can lead to increased intracellular probe transport. However, under physiological cell culture conditions, a very high concentration of 2-NBDG (up to 500 μM) was needed for achieving an acceptable signal-to-noise ratio in A549 cells (Fig. S7A). The same phenomenon has also been observed in other reported studies showing that extremely high concentration of 2-NBDG is needed in glucose containing cell culture systems.^[2,3] Furthermore, the fluorescence signals in cells treated with the highest concentration of 2-NBDG (500 μM) had been mostly quenched to undetectable levels due to the incompatibility of the probe with living cells (Fig. S7B).

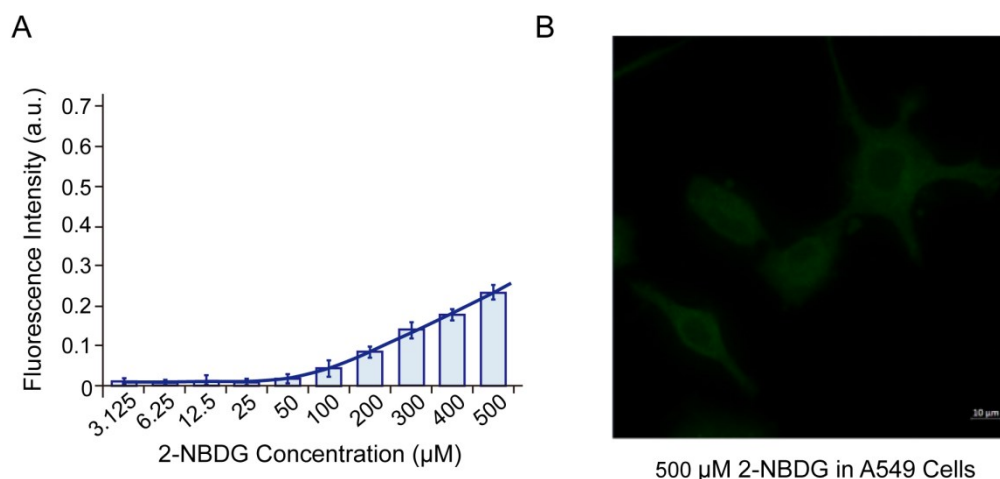


Figure S7. 2-NBDG uptake and accumulation in A549 cells. (A) Concentration dependent (3-500 μM) cellular uptake of 2-NBDG in A549 cells under physiological conditions for 1h. (B) Fluorescence microscopic imaging of 500 μM 2-NBDG labeled A549 cells at 3 h.

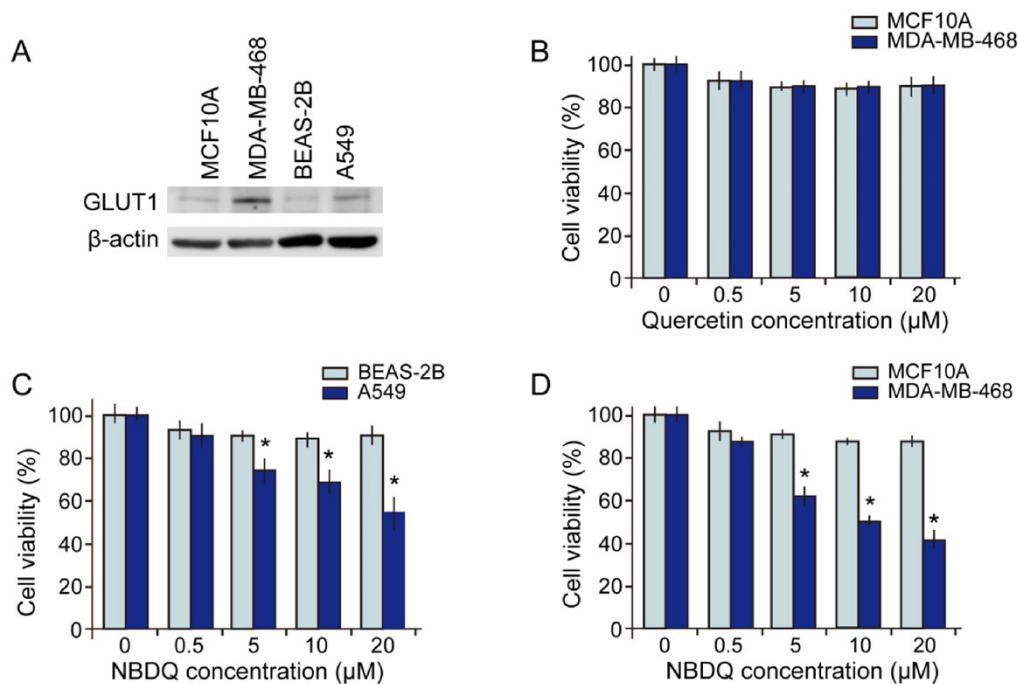


Figure S8. Cytotoxicity of Quercetin and NBDQ in Different Cell Lines. (A) The expression level of GLUT1 in non-small-cell lung cancer A549, normal bronchial epithelial BEAS-2B, TNBC MDA-MB-468 and non-tumorigenic human breast MCF10A cells. (B) 72 h cytotoxicity results for quercetin in human normal breast cell MCF10A and MDA-MB-468 TNBC cells from MTT assay. (C) 72 h cytotoxicity results for NBDQ in human normal bronchial epithelial BEAS-2B and A549 cells from MTT assay. (D) 72 h cytotoxicity results for NBDQ in human normal breast cell MCF10A and MDA-MB-468 TNBC cells from MTT assay. Data were presented as mean \pm S.E.M. *, $P < 0.01$; *t*-test.

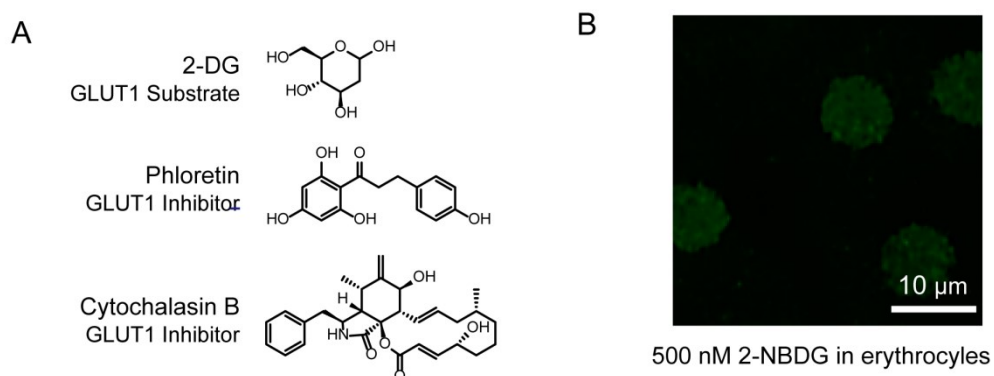


Figure S9. Known Inhibitors used for 2-DG Uptake Inhibition and Competition Assay. (A) Chemical structures of GLUT1 substrate 2-DG, flavonoid GLUT1 inhibitor Phloretin and GLUT1 specific inhibitor of natural mycotoxin Cytochalasin B. (B) Confocal fluorescence microscopy imaging of rat erythrocytes treated with 500 nM of 2-NBDG at 37 °C incubated for 30 min.

2-Deoxyglucose (2DG) Uptake with Inhibitor Combination. Human erythrocytes were used to evaluate the 2DG uptake influenced by different inhibitor combinations. The procedure was the same as described in the main text. Group-I: PBS buffer with 1 mM 2-deoxyglucose; Group-II: phloretin 200 μ M; Group-III: cytochalasin B 10 μ M; Group-IV: phloretin 200 μ M incubate for 60 min, then add NBDQ 10 μ M for another 60 min at 37°C; Group-V: CB 10 μ M incubate for 60 min, then NBDQ 10 μ M for another 60 min at 37°C. Percentage of 2DG uptake relative to the mean value of the control group were calculated for each inhibitor/combination.

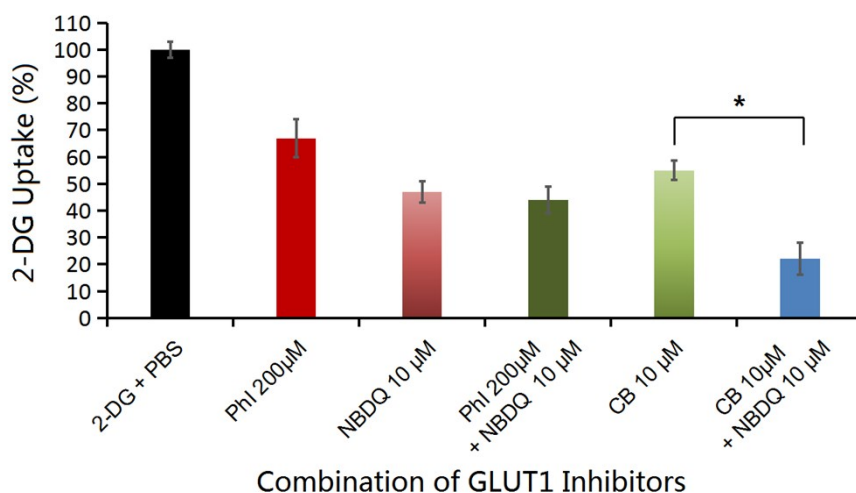


Figure S10. 2-Deoxyglucose (2DG) Uptake with Inhibitor Combination in Human Erythrocyte. PhI: phloretin, CB: cytochalasin B. *Significant from phloretin and cytochalasin B treated results at $P < 0.01$.

7. GLUT1 Inhibition Mechanism and Molecular Basis

Having shown the superiority of NBDQ over 2-NBDG in detecting tumors in TNBC and A549 xenograft mice, we proceeded to decipher the molecular basis of the binding modes of the rationally designed GLUT1 inhibitor NBDQ with the transmembrane protein. In order to do this, a long-time scale molecular dynamics simulation study was carried out utilizing YASARA as a robust molecular simulation tool (YASARA Biosciences. YASARA: Yet another scientific artificial reality application. <http://www.yasara.org/>) (See Supplementary, Fig. S8-S10, Table S2-S4). The 3D structure of GLUT1 was obtained from our previous reported GLUT1 study.^[4] NBDQ, phloretin, and quercetin were flexibly docked into the substrate binding site of GLUT1 using SurFlex-Dock GeomX protocol with SYBYL-X 2.0 software package. Take the docking results as the initial binding configuration of each molecule, 150 ns molecular dynamics simulations were performed with YASARA program. The MD simulation results as well as the binding mode of NBDQ with GLUT1 are shown in Fig. 9. The simulation results revealed that both NBDQ and phloretin share a similar binding site near the exofacial surface of the transporter, whereas quercetin lies in a different binding pocket near the central binding cavity (Fig. 9A-8D). The equilibrated binding location from our MD simulation for phloretin is consistent with the experimental results reported by Ojeda and Krupka's group, in which phloretin has been demonstrated to bind in a glucose competitive external site which alters the affinity of D-glucose on the external glucose binding.^[5,6] Our inhibitor competition assay clearly shows the competitive relationship between NBDQ and phloretin, therefore the MD simulation results validate our

competition results that the inhibitory effect of NBDQ on 2-DG uptake is due to the inhibitory binding of NBDQ with GLUT1 at an external binding site. To explain in greater detail for the binding mode, Phe291, Ile168, and Val69 form the main hydrophobic contact respectively with the aromatic moieties on the NBD- and quercetin-part of NBDQ molecule, while two single hydrogen bond interactions form from Asn317 and Gly314 with NBD, and one bridged hydrogen bond interaction occurs between the amide group of Gln283 and the quercetin phenol. These key interactions and binding mode represent the detailed molecular basis of the inhibitory action for NBDQ on GLUT1 (Fig. 9E).

Molecular Dynamics Simulations. GLUT1 3D structure was created following our previous reported method.^[4] Specifically, the glucose bound outward-facing GLUT1 was generated based on the crystal structure of XyIE (PDB ID: 4GBZ) and was used as initial 3D conformation for different inhibitor binding studies. Before MD simulation analysis, molecular docking studies were carried out after replacing each inhibitor with the central pocket bound glucose by using the docking module Surflex v.2.601 of SYBYL-X 2.0 platform.^[7,8] The docking mode was set to ultrafine GeomX. For protein preparation, all hydrogen atoms were added randomly, and side chains were optimized during the receptor preparation. In the docking process, the receptor was kept rigid and the optimized inhibitors were set to be flexible during docking.

After docking process completed, all systems were subjected to the MD simulation study. All MD simulations were performed using YASARA program.^[9] Firstly, the values of the nucleic acids' pK_a shifts were predicted,^[10] the protonation states were assigned according to $pH = 7.0$, and the simulation cell was filled with pure water.^[11] Prior to MD simulations, energy minimizations including steepest descent minimization and simulated annealing minimization were performed in water solvent. After minimization, the production simulation of 150 ns was then performed with the smooth particle-mesh Ewald (PME) method.^[12] The all-atom AMBER14 force field was used in our simulation.^[13] The value of non-bonded cutoff was set to 8.0 Å, the integration time step was set to 4 fs, and the constrained bonds were formed by the hydrogen atoms. The NPT ensemble (pressure P, temperature T, and number of atoms N) with the constant pressure of 1 atm and temperature of 298 K were used in this study.^[14] Molecular graphics and analysis of the simulation results were performed with the UCSF Chimera package.

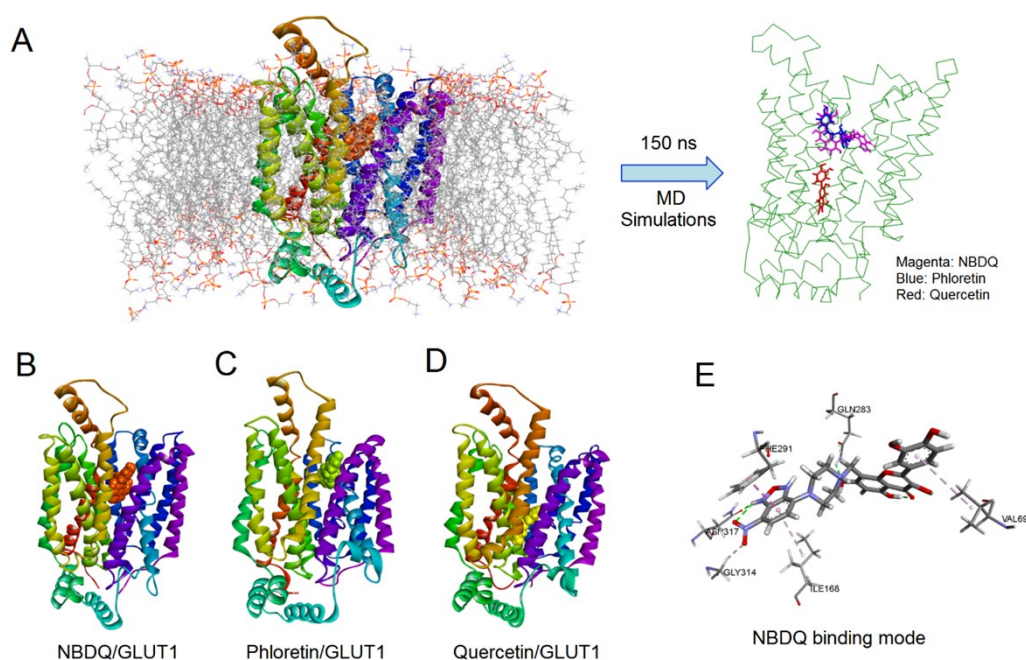


Fig. S11. Molecular dynamics simulations of hGLUT1 with GLUT1 inhibitor. (A) Molecular dynamics simulations of hGLUT1 embedded in a fully solvated palmitoyloleoylphosphatidylcholine (POPC) lipid bilayer with different inhibitors, and the binding locations resulted from a 150 ns MD study for NBDQ, Phloretin and Quercetin. (B) (C) (D) Equilibrated structures of the inhibitor-bound GLUT1 transmembrane protein after 150 ns MD simulations for NBDQ, Phloretin and Quercetin. (E) Binding mode and key interactions of NBDQ within GLUT1 extracted from MD simulation result.

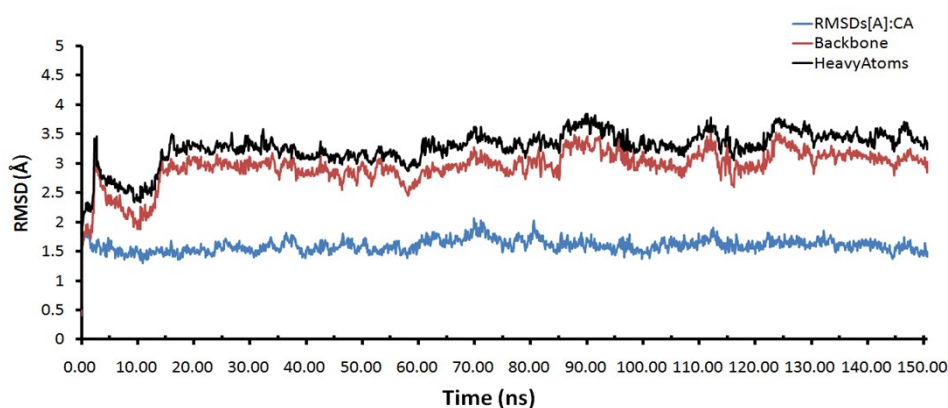


Figure S12. Root mean square deviation (RMSD) fluctuations of 150 ns MD simulations for NBDQ-bound hGLUT1 embedded in a fully solvated palmitoyloleoylphosphatidylcholine (POPC) lipid bilayer.

Table S1. Summary of 150 ns MD simulation results for NBDQ-bound hGLUT1 complex.

	Energy[kJ/mol]							RMSDs[Å]		
	Total	Bond	Angle	Dihedral	Planarity	Coulomb	VdW	Ca	Backbone	HeavyAtoms
Mean	-584605.01	79470.41	79357.411	187884.381	941.05	-978455.84	46197.574	1.597	2.937	3.266
Min	-827604.08	13233.389	19678.097	179151.804	235.973	-1124613.4	41924.989	0.403	0.436	0.516
Max	-572323.92	82320.341	81687.274	190701.591	1074.112	-959143.83	84710.101	2.062	3.6	3.847

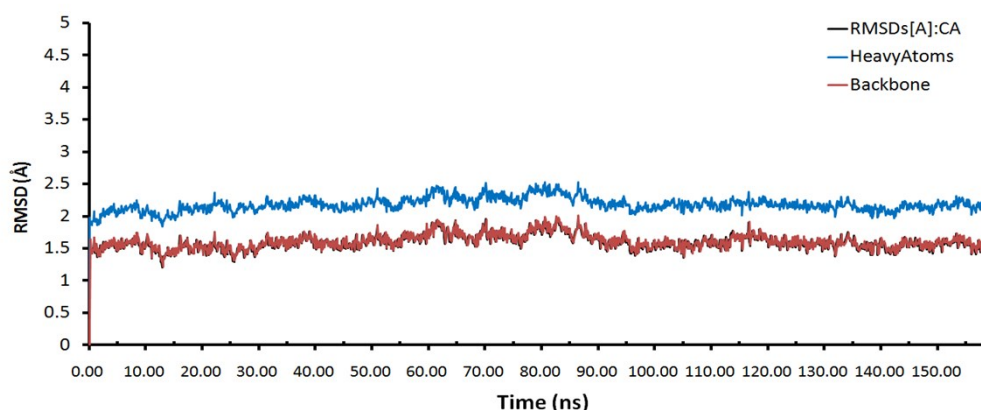


Figure S13. Root mean square deviation (RMSD) fluctuations of 150 ns MD simulations for Phloretin-bound hGLUT1 embedded in a fully solvated palmitoylcholine (POPC) lipid bilayer.

Table S2. Summary of 150 ns MD simulation results for Phloretin-bound hGLUT1 complex.

	Energy[kJ/mol]							RMSDs[Å]		
	Total	Bond	Angle	Dihedral	Planarity	Coulomb	VdW	CA	Backbone	HeavyAtoms
Mean	-605028.27	81279.71	80283.565	188604.74	930.678	-1006037.6	49910.686	1.598	1.605	2.181
Min	-856845.02	13268.641	18628.452	179376.43	225.779	-1159738	46622.071	0.375	0.407	0.499
Max	-594196.96	85131.277	82654.688	190315.9	1065.25	-992045.52	91393.646	2.006	2.008	2.531

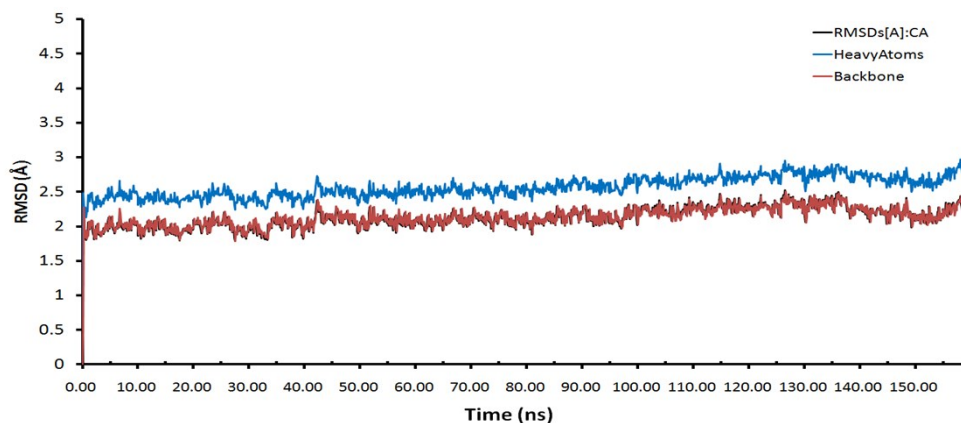


Figure S14. Root mean square deviation (RMSD) fluctuations of 150 ns MD simulations for Quercetin-bound hGLUT1 embedded in a fully solvated palmitoylcholine (POPC) lipid bilayer.

Table S3. Summary of 150 ns MD simulation results for Quercetin-bound hGLUT1 complex.

	Energy[kJ/mol]							RMSDs[Å]		
	Total	Bond	Angle	Dihedral	Planarity	Coulomb	VdW	CA	Backbone	HeavyAtoms
Mean	-622116.585	82833.431	80951.856	188969.341	929.05	-1028966.204	53165.941	2.13	2.134	2.567
Min	-880098.316	24005.72	18421.799	179564.168	235.679	-1199188.039	49742.138	0.418	0.451	0.52
Max	-611690.198	96581.661	82900.966	190538.287	1060.925	-1014725.098	96862.358	2.525	2.511	2.974

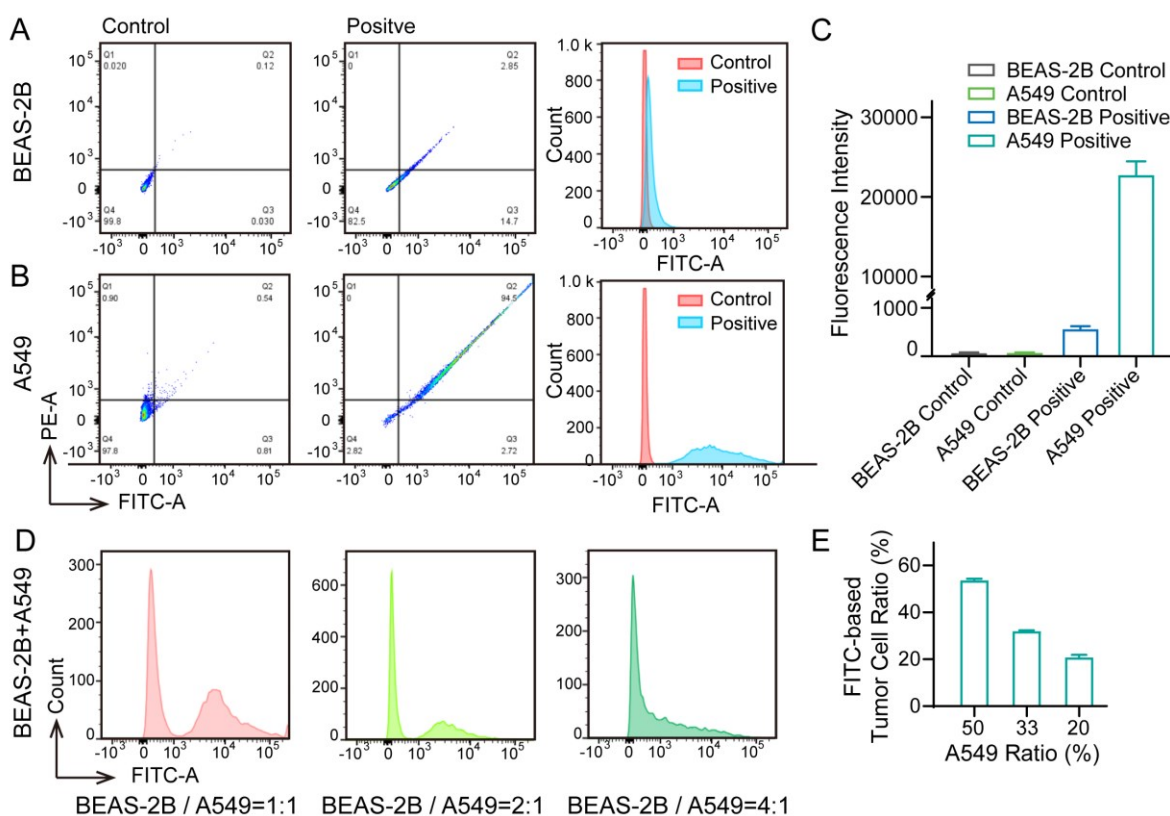


Figure S15. (A, B) Flow cytometry scatter plots and corresponding histograms of BEAS-2B and A549 cells fluorescence intensity in control or positive (treated with 50 μ M NBDQ) samples. (C) The fluorescence intensity of cells in each group. (D) Histogram of differentiation and quantification results of different ratio of BEAS-2B and A549 cells treated with NBDQ. (E) Quantitative analysis results based on fluorescence intensity of the mixed cells. Data were presented as mean \pm S.E.M.

Table S4. Tumor-to-background ration (Tm/Bkg) and tumot-to-organ ratio (Tm/Org) for NBDQ and 2-NBDG treated TNBC bearing xenograft mice.

□	NBDQ				2-NBDG		
	6 h	12 h	24 h	72 h	6 h	12 h	24 h
Tm/Bkg ^a	12.37 \pm 2.02	11.02 \pm 2.11	9.56 \pm 1.52	7.73 \pm 0.93	5.44 \pm 1.06	0.62 \pm 0.10	0.39 \pm 0.05
Tm/Org ^b	8.60 (at 72 h)				3.48 (at 24 h)		

^a Based on fluorescence intensity of tumor (FI_{tumor}) and background (FI_{bkg}) measured from living animals for each time point. ^b Based on average fluorescence intensity of tumor (FI_{tumor}) and of the selected organs (FI_{org}) measured from *ex vivo* samples (n=3).

8. *In Vivo* Fluorescence Imaging of NBDQ in A549 Xenograft Mice

In addition to TNBC, the effect of NBDQ for A549 xenograft tumor imaging was also evaluated following the same method. Under unfasted conditions, NBDQ achieved similar results with pronounced imaging efficiency against the GLUT1 high expression A549 tumors. Excellent biocompatibility with up to 72 h long-lasting signal persistence with a highest image contrast of $Tm/Org = 8.44$ have been observed for NBDQ in A549 xenograft tumor imaging (Fig. 8A-B, Table S1). The tumor-to-organ ratios for groups of mice ($n=3$) was recorded as 4.71 (Fig. 8C, Table S1). Based on the literature reports, similar animal studies, if under unfasted conditions, ^{18}F -FDG uptake could only afford a tumor-to-organ ratio of 1.37 : 1 for human epidermal carcinoma A431 and 2.02 : 1 for human glioma U251 xenograft mice since plasma glucose with normal feeding will significantly reduce the tumor ^{18}F -FDG uptake and disturb glucose metabolic activity.^[15]

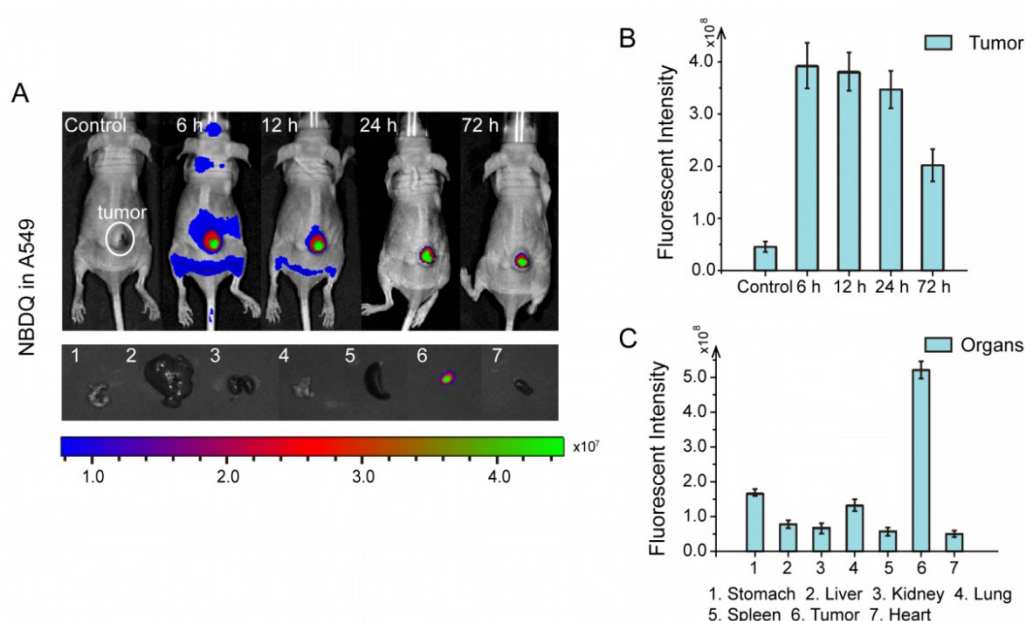


Fig. S16. *In vivo* imaging for NBDQ treated A549 xenograft mice. (A) *In vivo* imaging and the *ex vivo* optical images of organs for NBDQ treated A549 xenograft mice. Up to 72 h following administration of 0.2 $\mu\text{mol}/\text{mouse}$ of the probe under *ad libidum* feeding conditions. White circle indicates the location of the tumor. (B) Quantitative analysis of mean fluorescence intensity of NBDQ determined over time by measurement of respective tumor regions of interest, (averaged from $n=3$). (C) The quantitative biodistribution of NBDQ from *ex vivo* tumor tissues and organs ($n=3$, at 72 h). λ_{ex} . 470 ± 10 nm and λ_{em} . 565 ± 20 nm.

Table S5. Tumor-to-background ration (Tm/Bkg) and tumot-to-organ ratio (Tm/Org) for NBDQ treated A549 bearing xenograft mice.

NBDQ Treated A549 Xenograft Mice				
Time	6 h	12 h	24 h	72 h
Tm/Bkg^a	8.44 ± 1.27	8.34 ± 2.03	7.51 ± 1.33	4.61 ± 0.55
Tm/Org^b	□ 4.71 (at 72 h)			

^a Based on fluorescence intensity of tumor (FI_{tumor}) and background (FI_{bkg}) measured from living animals for each time point. ^b Based on average fluorescence intensity of tumor (FI_{tumor}) and of the selected organs (FI_{org}) measured from *ex vivo* samples ($n=3$).

9. *In Vivo* Efficacy Study of NBDQ in MDA-MB-468 Xenograft Mice

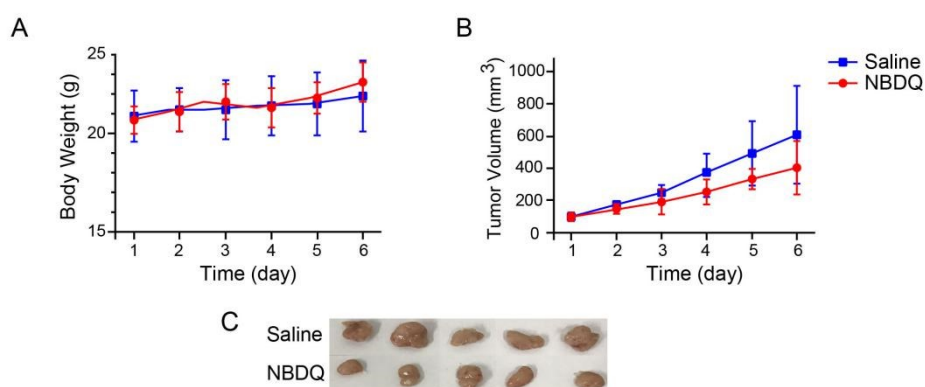


Fig. S17. *In vivo* antitumor efficacy for NBDQ treated MDA-MB-468 xenograft mice. (A) Averaged body weight changes during the treatment. (B) Suppression of tumor growth with NBDQ treatment. 5 female BALB/c nude mice were used for both saline and NBDQ group. 10 mg/kg of NBDQ was dosed by tail vein injection (10 mL/kg) daily for 6 days.

10. Original Gels of the Western Blot

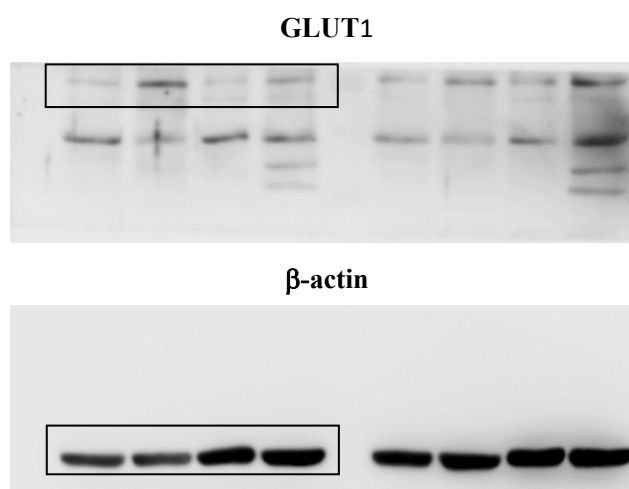


Fig. S18. Raw images for Fig. 1B & Figure S8A (the same graph for GLUT1 expression). Top and bottom images are in the same plate. β-Actin staining was obtained after removing of GLUT1 recognizing antibodies with stripping buffer.

11. References

- [1] C. Zou, Y. Wang, Z.J. Shen, 2-NBDG as a fluorescent indicator for direct glucose uptake measurement, *Biochem. Biophys. Methods* 64 (2005) 207-215.
- [2] X. Gao, S. Liu, Y. Shi, Z. Huang, Y. Mi, Q. Mi, et al., Mechanistic and biological characteristics of different sugar conjugated 2-methyl malonato-platinum(II) complexes as new tumor targeting agents, *Eur. J. Med. Chem*

125 (2017) 372-384.

- [3] K. Ohtsubo, S. Takamatsu, M.T. Minowa, A. Yoshida, M. Takeuchi, J.D. Marth, Dietary and Genetic Control of Glucose Transporter 2 Glycosylation Promotes Insulin Secretion in Suppressing Diabetes, *Cell* 123 (2005) 1307-1321.
- [4] X. Fu, G. Zhang, R. Liu, J. Wei, D. Zhang-Negrerie, X. Jian, et al., Mechanistic Study of Human Glucose Transport Mediated by GLUT1, *J. Chem. Inf. Model* 56 (2016) 517-526.
- [5] P. Ojeda, A. Pérez, L. Ojeda, M. Vargas-Uribe, C.I. Rivas, M. Salas, et al., Noncompetitive blocking of human GLUT1 hexose transporter by methylxanthines reveals an exofacial regulatory binding site, *Am. J. Physiol. Cell Physiol* 303 (2012) C530-C539.
- [6] R.M. Krupka, Asymmetrical binding of phloretin to the glucose transport system of human erythrocytes, *J. Membr. Biol* 83 (1985) 71-80.
- [7] Jain A. N.; Surfex: fully automatic flexible molecular docking using a molecular similarity-based search engine. *J. Med. Chem.* 2003, 46, 499–511.
- [8] Ruppert J.; Welch W.; Jain A. N. Automatic identification and representation of protein binding sites for molecular docking. *Protein Sci.* 1997, 6, 524-533.
- [9] Krieger E.; Koraimann G.; Vriend G. Increasing the precision of comparative models with YASARA NOVA: a self-parameterizing force field. *Proteins* 2002, 47, 393–402 (2002).
- [10] Krieger, E.; Nielsen, J. E.; Spronk, C. A. E. M.; Vriend, G. Fast empirical pKa prediction by Ewald summation. *J. Mol. Graph. Model.* 2006, 25, 481-486.
- [11] Krieger, E.; Darden, T.; Nabuurs, S. B.; Finkelstein, A.; Vriend G. Making optimal use of empirical energy functions: Force-field parameterization in crystal space. *Proteins* 2004, 57, 678-683.
- [12] Cheatham, T. E.; Miller, J. L.; Fox, T.; Darden, T. A.; Kollman, P. A. Molecular Dynamics Simulations on Solvated Biomolecular Systems: the Particle Mesh Ewald Method Leads to Stable Trajectories of DNA, RNA, and Proteins. *J. Am. Chem. Soc.* 1995, 117, 4193–4194.
- [13] Galindo-Murillo, R.; Robertson, J. C.; Zgarbova, M.; Spomer, J.; Otyepka, M.; Jurecka, P.; Cheatham, T. E. Assessing the Current State of Amber Force Field Modifications for DNA. *J. Chem. Theory Comput.* 2016, 12, 4114–4127.
- [14] Krieger, E.; Vriend, G. New ways to boost molecular dynamics simulations. *J. Comput. Chem.* 2015, 36, 996-1007.
- [15] B.J. Fueger, J. Czernin, I. Hildebrandt, C. Tran, B.S. Halpern, D. Stout, et al., Impact of Animal Handling on the Results of 18F-FDG PET Studies in Mice, *J. Nucl. Med* 47 (2006) 999-1006.